Chin. Geogra. Sci. 2019 Vol. 29 No. 4 pp. 626–639
https://doi.org/10.1007/s11769-019-1060-0

Springer Science Press
www.springerlink.com/content/1002-0063

Exploring the Potential of Mapping Cropping Patterns on Smallholder Scale Croplands Using Sentinel-1 SAR Data

Juliana USEYA, CHEN Shengbo

(*College of GeoExploration Science and Information Engineering*, *Jilin University*, *Changchun* 130026, *China*)

Abstract: It is of paramount importance to have sustainable agriculture since agriculture is the backbone of many nations' economic development. Majority of agricultural professionals rarely capture the cropping patterns necessary to promote Good Agricultural Practises. Objective of this research is to explore the potential of mapping cropping patterns occurring on different field parcels on small-scale farmlands in Zimbabwe. The first study location under investigation are the International Maize and Wheat Improvement Center (CIMMYT) research station and a few neighboring fields, the second is Middle Sabi Estate. Fourier time series modeling was implemented to determine the trends befalling on the two study sites. Results reveal that Sentinel-1 synthetic aperture radar (SAR) time series allow detection of subtle changes that occur to the crops and fields respectively, hence can be utilized to detect cropping patterns on small-scale farmlands. Discrimination of the main crops (maize and soybean) grown at CIMMYT was possible, and crop rotation was synthesized where sowing starts in November. A single cropping of early and late crops was observed, there were no winter crops planted during the investigation period. At Middle Sabi Estate, single cropping on perennial sugarcane fields and triple cropping of fields growing leafy vegetables, tomatoes and onions were observed. Classification of stacked images was used to derive the crop rotation maps representing what is practised at the farming lands. Random forest classification of the multi-temporal image stacks achieved overall accuracies of 99% and 95% on the respective study sites. In conclusion, Sentinel-1 time series can be implemented effectively to map the cropping patterns and crop rotations occurring on small-scale farming land. We recommend the use of Sentinel-1 SAR multi-temporal data to spatially explicitly map cropping patterns of single-, double- and triple-cropping systems on both small-scale and large-scale farming areas to ensure food security.

Keywords: cropping patterns; polarized backscatter; time series; Sentinel-1 SAR; Zimbabwe

Citation: Juliana USEYA, CHEN Shengbo, 2019. Exploring the Potential of Mapping Cropping Patterns on Smallholder Scale Croplands Using Sentinel-1 SAR Data. *Chinese Geographical Science*, 29(4): 626–639. https://doi.org/10.1007/s11769-019-1060-0

1 Introduction

Sustainability of agricultural systems in both developing and developed countries can benefit a lot from Cropping Systems Analysis (Sharma et al., 2011). Endeavoring to guide the production systems towards sustainable agriculture, Good Agricultural Practices (GAP) are crucial. Proper GAP contribute to food security by generating income through the access to market and improve the working conditions of producers and their families. Therefore, GAP are everyone's responsibility and enable provision and attainability of harmless agricultural products of high quality. At the bottom of the chain commences with good cropping practices. It is fundamental to determine and understand the cropping practices to map croplands precisely (Bégué et al., 2018). Nevertheless, Bégué et al. (2018) gave a detailed typology of cropping practices and their definitions, since agronomic-related vocabulary sometimes lacks precision in the remote sensing literature.

Received date: 2018-08-08; accepted date: 2018-12-03

Foundation item: Under the auspices of Fundamental Research Funds for the Central Universities, China (No. 2017TD-26), the Plan for Changbai Mountain Scholars of Jilin Province, China (No. JJLZ[2015]54)

Corresponding authors: Juliana USEYA. E-mail: julieuseya@yahoo.co.uk; CHEN Shengbo. E-mail : chensb@jlu.edu.cn

An important indicator of the performance of an agricultural system and the adaptivity of an agricultural society is the measure of cropping systems diversity (Dimov et al., 2016). Crop diversification is a crucial instrument for economic growth (Bharati et al., 2015). Diversity of crops can be examined using several methods. Several crops cultivated and proportion of area under various crops can be used as a simple measure of diversity (Bharati et al., 2015). Since the determination of crop diversity indices requires a long-term inventory of crop maps, remote sensing can be the best tool to provide this kind of information.

Remote sensing is ubiquitous and contributes immensely to the mapping of both small and large regions of land under agricultural crop production. Jackson (1984) and Moran et al. (2012) highlighted that farm management could be enhanced by utilizing satellite imagery since it has a unique and crucial role in monitoring crops. Satellites have an advantage of their ability to generate synoptic, systematic, and repetitive coverage of a large area within a short period and provide information about the crops. Yan et al. (2014) utilized MODIS EVI (Enhanced Vegetation Index) time series data to delineate the dynamics of double- and triple-cropping practices. However, MODIS data is available at a moderate spatial resolution of 500 m, which might not be suitable to map small fields at small farming scales.

Remote sensing is a useful tool for providing updated information about agricultural cropping patterns, intensity, and land use. Precise agricultural information is of vital importance in monitoring changes in cropping systems and measure reactions of farmers to climate change issues (Forkuor et al., 2014). Conversely, discrimination of crops can be a considerable challenge when this information is being derived from optical systems that rely on Sun's energy since consistent image acquisition in hazy or cloudy conditions can be erratic despite the wide availability of an increased number of satellites with high temporal resolution. Synthetic Aperture Radar (SAR) systems possess acquisition capabilities that are independent of weather conditions and daylight, hence they can offer more reliable, dependable, and usable radar images compared to optical images. Moreover, to avert clouds from lowering accuracy, microwave images produced by SAR have been used for crop classification in many scenarios (Hütt and Waldhoff, 2018).

Although radar imagery is almost or entirely not affected by cloud coverage and atmospheric conditions, it is influenced by speckle noise. When detecting specific materials and surfaces, the presence of speckle can be advantageous, when supported by the analysis of noise patterns and disturbances. In most cases, however, speckle noise is desired to be reduced through filtering to derive more precise information from the SAR image (Dimov et al., 2016). Many spatial filters have since been developed which aim to effectively reduce speckle in radar images without eliminating the fine details, namely the Lee Filter, the Frost Filter and the popular Lee Sigma Filter (Portnoi, 2017). It is crucial to apply a polarimetric speckle filter before analysis to achieve reliable results (Portnoi, 2017).

The acquisition of SAR imagery at intervals during the growing season, can facilitate accurate crop discrimination (Foody et al., 1994). The structure of a canopy is different among crops and inescapably change as crops grow. SAR responds very well to the structural differences, and that is how these sensors can accurately detect crop type and have proven sensitive to several crop biophysical parameters (McNairn and Shang, 2016). SAR data have great potential and can be utilized by different agricultural professionals that deal with day-to-day decision making in agricultural management. Upon fully realizing the potentials offered by SAR, it will immensely improve the administration of activities in the agricultural sector.

There is a research conducted utilizing Sentinel-1 by Mattia et al. (2015), but the mapping was done at high spatial resolution (e.g., 100–500 m). Results indicated a good agreement with the actual distribution of cereal crops in the area but of the cereal's class, wheat, barley, and oats could not be separated/distinguished. Contrariwise, authors such as Martínez and Martín (2003) and Jackson (1984) believed that there was an underutilization of remote sensing data in agricultural applications in map long term cropping patterns and crop rotations. According to a detailed literature analysis done by Bégué et al. (2018), less than 10% of the publications on remote sensing and agriculture focus on cropping practices.

Agriculture is the backbone of Zimbabwe's economy where small-scale farmers are the significant players in agricultural production. Most of the Zimbabwean cultivated fields are small and heterogeneous fields on a fragmented landscape that require high spatial resolution imagery to map them accurately. There is a lack of spa-

tially explicit information regarding cropping patterns crucial for inventory purposes. The cropping patterns can be derived from the spatial distribution and phenological characteristics of crops. Due to an inexorable cloud problem, the use of optical imagery hinders their application in mapping. Therefore the use of radar SAR imagery becomes apparent. Therefore, this paper's main objective is to explore the potential of utilizing Sentinel-1 SAR data to map cropping patterns at two sites namely International Maize and Wheat Improvement Center (CIMMYT) research institute and a few neighboring fields in Harare and Middle Sabi Estate in Chipinge District, Zimbabwe. The spatially explicit mapping of cropping patterns can assist in preparing an inventory of what was grown, where and when, and is vital for the tracking of land and water resources necessary for crop production over space and time. Double- and triple-cropping per year is crucial in meeting the escalating food demand (Yan et al., 2014) all over the world. Knowledge of cropping intensities is crucial to understand water requirements necessary for water resources management (Heller et al., 2012).

2 Study Area and Data

2.1 Study area

Two study sites were chosen for this research, the first location is CIMMYT research station and a few neighboring fields situated in Harare, Zimbabwe bounded by 17°43′14″E and 17°44′16″E, 30°59′40″S and 31°15′00″S with an average altitude of 1489 m (Fig. 1a). It is situated in agro-ecological zone IIA, meaning that it receives moderately high rainfall during summer ranging between 750 and 1000 mm/yr (Mukwada and Manatsa, 2013). CIMMYT generally works throughout the developing world to improve livelihoods and foster more productive sustainable maize and wheat farming. It targets critical challenges, including food insecurity and malnutrition, climate change, and environmental degradation (CIMMYT, 2016). Generally, at this site, they grow seasonal crops mainly maize, soybean, and wheat.

The second study site is Middle Sabi Estates in Chipinge district, Zimbabwe, bounded by latitudes of 20º08′12″E and 20º23′38″E and longitudes 32º18′07″S and 32º23′58″S (Fig. 1b). It is situated in agro-ecological region zone IV, which is a semi-intensive farming region. It receives relatively low rainfall totaling between 450 and 650 mm/yr (Mukwada and Manatsa 2013). The farming system in this region is mostly based on livestock production, but it can be intensified to some extent by the growing of drought-tolerant fodder crops. Precisely, the vast land at this site, there is mono-cropping of sugarcane. The sugarcane grown at Middle Sabi Estate is mainly used to produce the best performing fuel from anhydrous ethanol with less than 0.04% water content (http://www.greenfuel.co.zw/).

Zimbabwe is a landlocked country in the Southern part of Africa and is generally an agricultural based country with a well-developed and diversified agricultural sector producing food crops and cash crops. As of 2015, agriculture accounted for 18% of Zimbabwe's gross domestic product (GDP) (Dzirutwe, 2015). Zimbabwe has two distinct seasons, namely summer and winter. Usually, a typical long rainy season generally falls between October and April, whereas winter season falls between June and August. However, the dry season begins from April until September. Zimbabwe has a temperate climate.

Major crops grown in summer are usually planted around October or November, depending on the onset of the rains. These include maize, soybean, cotton, and tobacco. Wheat is the major winter crop grown in Zimbabwe. Small-scale farmers are the backbone of the country's food security and provide about 70 percent of maize (Toringepi, 2016), which is the country's staple food. Small-scale sugarcane producers team up and grow the crop on the same area since it requires full irrigation to grow. The small-scale farmers usually practice crop rotation of their farms necessary for conservation agriculture (Marongwe et al., 2011). Due to economic hardships, most farmers tend to grow cash crops often.

2.2 Data

2.2.1 Sentinel-1 SAR Data

Sentinel-1 (S1) is a modern C-band imaging radar constellation of two satellite, S1A, and S1B that were launched in 2014 and 2016 respectively with dual-polarization capability (HH+HV or VV+VH) for earth observation. It is representing the first sensor designed for the EU/ESA Copernicus Project initiated by the European Union. The Sentinel-1 SAR imagery is available in four exclusive imaging modes, namely Wave-Mode (WM), Extra-

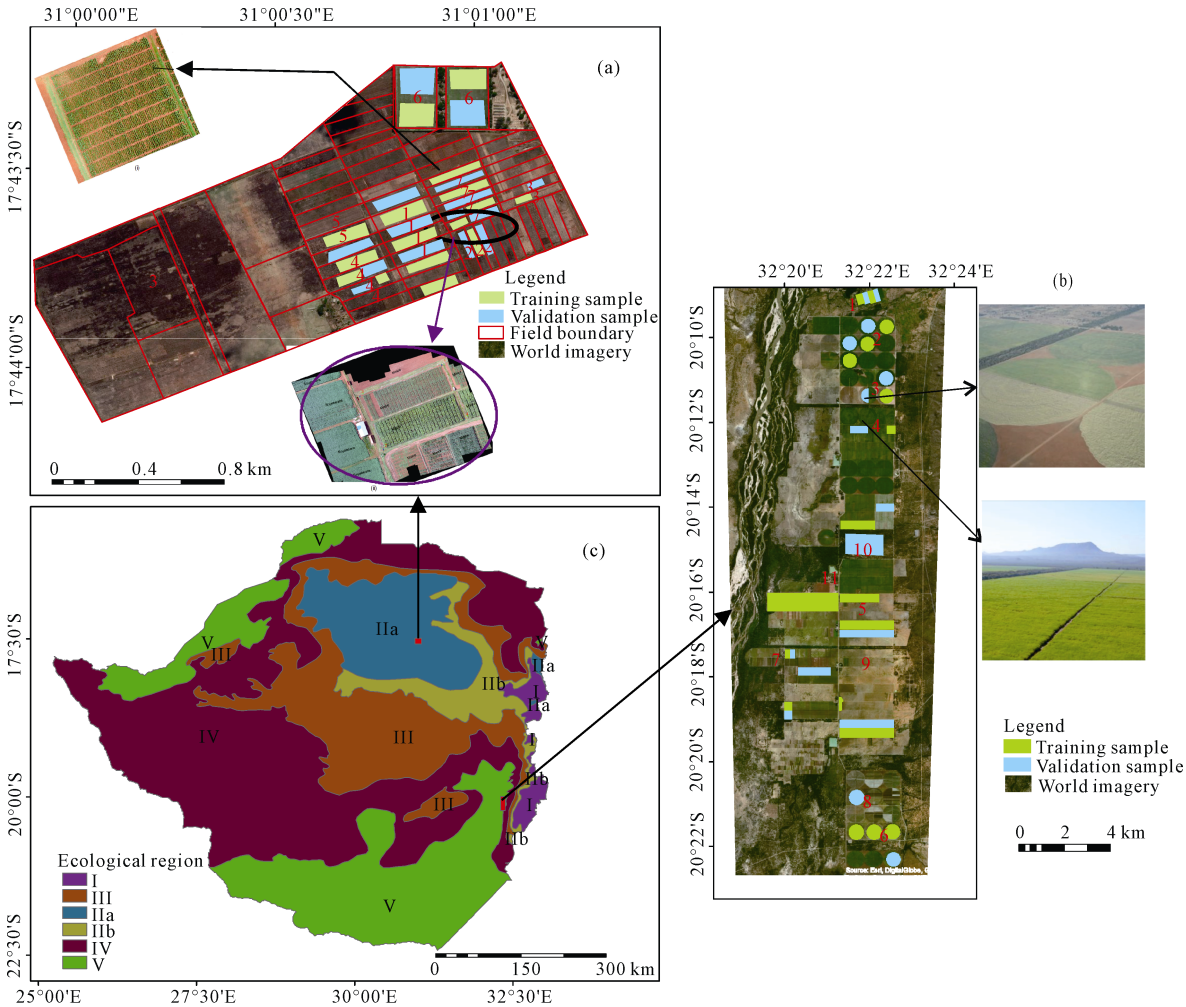

Fig. 1 Locations of study sites (a) CIMMYT, Harare showing training and validation data and corresponding UAV images collected on 3rd December 2016 and 9th of February 2018 (where 1 represent soybean fields, 2, 5, 7 are maize fields, 3 are fields of mixed crops, 4 are fallow fields, and 6 are areas for pasture), (b) Middle Sabi Estate in Chipinge showing training and validation samples and UAV images showing center pivot irrigation and sprinkler irrigation on rectangular fields (where 1 represents banana field, 2, 3, 6, and 8 are sugarcane fields, 4 and 9 are fallow fields, 5 is a vegetable field, 7 is orchard, 10 is a tree plantation, and 11 is a waterbody), (c) Ecological regions map of Zimbabwe

Wide Swath Mode (EW), Interferometric Wide Swath Mode (IW) and Strip Map Mode (SM). It provides free data access and unprecedented high temporal resolution, which enables new possibilities to capture the dynamics in agricultural areas using multi-temporal classification approaches that include information about the crops' phenology (Bargiel, 2017). S1 SAR mission is that the satellite is mainly operated in the Terrain Observation with Progressive Scans (TOPS) mode (Wegmüller et al., 2016).

Level-1 Ground Range Detected (GRD) Sentinel-1 C-band (5.405 GHz) images in Interferometric Wide swath (IW) mode, are downloaded from the Sentinel data hub, scihub.copernius.eu website. IW mode allows the combination of a large swath width (250 km) with a moderate geometric resolution (10 m). The provided GRD products contain amplitude and intensity images in each polarization (VH and/or VV) with level 1 processing which includes data projected to ground range using an Earth ellipsoid model, elevation antenna pattern and range spreading loss corrections and thermal noise removal (Suresh et al., 2016). The IW image with incidence angle varying from 30° to 45° and pixel spacing of 10 m in both range and azimuth.

At CIMMYT and surrounding fields, a total of 30 SAR images with dates ranging from October 2016 up to February 2018 were used for time series to investigate the multi-temporal backscatter properties. At Mid-

dle Sabi Estate, 33 SAR images from January 2016 to January 2018 were used.

2.2.2 Reference samples and ancillary data

Reference data for CIMMYT site were availed to authors in the form of georeferenced, mosaicked UAV images by the personnel at the research station. Fig. 1a shows UAV images captured on the 3rd December 2016 and 9th February 2018. At Middle Sabi Estate, the UAV images (Fig. 1b) were obtained from Green Fuel's website http://www.greenfuel.co.zw/gallery/.

Ancillary data comprised of farm records from both study sites, which was availed to the authors by authorities of the organizations. The farm records contain attribute information regarding the crop(s) planted on each field/parcel/section for each season but did not provide planting dates nor harvest dates. Training and validation samples shown in Figs. 1a, 1b were selected using the information extracted from both farm records and UAV images of research site and estate. The farm records are very critical for this research to assist in the classification or analysis.

3 Methodology

3.1 SAR Image pre-processing

Pre-processing of SAR imagery takes a significant part because the aim is to derive the actual intensity of the emitted microwave signal that is received by the sensor (Dimov et al., 2016). The image processing steps were performed in ESA's Sentinel Application Platform (SNAP) starting with radiometric correction, speckle filtering, geocoding and geometric terrain correction. SRTM 3sec was used as the Digital Elevation Model. All the images were then co-registered into WGS84/ UTM Zone 36S coordinate system.

3.1.1 Speckle filtering

Pixels contain many point scatterers (Lopes et al., 1993) that alter reflected backscatter into different phases, and it cascades to interference and the noise-like effect known as speckle. Speckle filtering suppresses the noise to allow better interpretation and backscatter analysis. However, speckle filters do not only suppress the noise but also remove observations that are not affected by noise and contain valuable land surface information (e.g., soil moisture, biomass, hence resulting in a loss of spatial resolution since it is carried out with moving windows. Speckle in SAR reduces classification accuracy (Geetha et al., 2016). Therefore, the selection of filter to use is an important step, a filter that reduces speckle in radar images without eliminating the fine details. For this paper, Lee filter (Lee et al., 1994; Nyoungui et al., 2002; Ozdarici and Akyurek, 2010) was chosen with a moving window of 3 × 3 kernel since the study areas are relatively small.

3.1.2 Conversion from intensity to decibel

A SAR system records the echo received from a transmitted electromagnetic signal in the form of intensity per pixel (Portnoi, 2017). The intensity values have to be converted to a physical quantity known as the backscattering coefficient. To get better constraints, conversion from intensity σ^0 to σ^0 (dB) is a crucial step. Thus, the σ^0 values of the SAR image are then converted to Decibels (dB) (σ^0 is the radar backscatter per unit area.) The images in dB were then georeferenced to UTM zone 36S. The linear conversion formula (radar equation) presented by Crawford and Ricard (1998) is as shown by Equation (1):

$$\sigma^0 = \sigma_m^0 \frac{10\log_{10}}{\theta_n}\theta \tag{1}$$

where σ^0 is scattering coefficient, σ_m^0 is the maximum value for the scattering coefficient (usually measured at vertical incidence), θ is the angle of incidence and θ_0 is a constant dependent on terrain type frequency and polarization.

A linear correction is applied at each frequency and polarization to generate uniform backscatter statistics for a given class (Crawford and Ricard, 1998).

3.2 Post-processing

The post-processing stage involves subset, co-registration and data stacking, visualization of data, and calculation of image statistics. Creation of subset images, co-registration, and stacking were performed in SNAP.

Co-registration refers to the spatial alignment of a series of images. Stacking is a component of co-registration where two or more spatially overlapping products are collocated. No resampling method was implemented since the master image's extent is adopted for the output image. The collocation algorithm iterates over all the pixels in the master products and tries to find the closest pixel in the slave product. The pixels in slave images are moved to align with the master image to sub-pixel ac-

curacy (Veci, 2016). The time series images are co-registered into a stack in order of their acquisition dates, thus creating a multilayer image from a set of individual subset images from the step above.

3.3 Crop types discrimination and cropping patterns using Fourier time series

Crops typically exhibit a temporally varying backscatter signal due to their phenological interaction with the microwave signal (Nguyen et al., 2015). Time series plots are ideal for understanding the changes that occur within and between seasons (permanent, summer and winter crops), and between classes within the various classes. Various fields or sections at the farms were chosen. The random selection of sample pixels and the collection of their statistical values was done in SNAP. Average backscatter values of the various fields corresponding to various dates were exported to Matlab and used for time series analysis.

Fourier series was implemented for curve fitting and smoothing purposes (de Oliveira et al., 2009). One of the advantages of Fourier series is that it deals with time series of irregularly spaced observations. Fourier series is a sum of sine and cosine functions that describes a periodic signal. It is represented in either the trigonometric form of the exponential form. Trigonometric Fourier series function equation as shown by Equation (2).

$$y = a_0 + \sum_{i=a}^{n} a_i \cos(iwx) + b_i \sin(iwx) \tag{2}$$

where a_0 models a constant (intercept) term in the data and is associated with the $i = 0$ cosine term, w is the fundamental frequency of the signal, n is the number of terms (harmonics) in the series and $1 \leq n \leq 8$. Fourier series modeling was implemented in Matlab.

3.4 Image classification

Both single date and stacked S1 SAR images were classified using both *K*-means and Random Forest (RF) classification algorithms in SNAP. *K*-means clustering algorithm (Doukkali, 2017) is an unsupervised classification method that requires identification of cluster centroids, depending on the points involved. Therefore, it aims at assigning n observation into k clusters whereby each point belongs to a cluster with the nearest mean. For this research, for CIMMYT images, 10 classes were randomly assigned as the initial number of classes ($k = 10$), after taking into consideration that the training samples have an average of seven classes. There exist initialization methods such as Random partition and Forgy methods which can also be implemented to choose the initial number of classes.[①] The value of k is reduced after every run until $k = 5$. Depending on the results obtained, the setup with the highest classification accuracy was adopted.

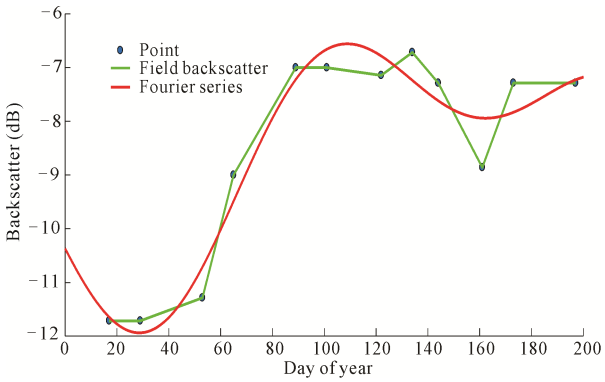

Fig. 2 Fourier series performance when smoothing the backscatter

For Middle Sabi Estate images, initial $k = 15$ was chosen, and value of k was reduced after every run until $k = 6$. Setup with the highest classification accuracy was adopted.

RF (Breiman, 2001) is a supervised ensemble classification method that considers a forest of randomized trees in a random composition of single decision trees that try to find the best fit between the original and the sampling data (Dimov et al., 2016). RF utilizes bootstrap aggregation (iterative bagging) operation where the number of trees (*ntree*) are independently built using a random subset of samples from the training data. For all datasets, 300 trees were employed.

Overall classification accuracies and kappa coefficients were obtained from the confusion matrices. F1 scores were calculated from producer's and user's accuracies.

① https://www.cse.iitb.ac.in/~shivaram/teaching/old/cs344+386-s2017/resources/la-5/lab-assignment-5.html

3.5 F1 test

F1 test was conducted to determine the F1-score values calculated from producer's and user's accuracies of each class as obtained from the confusion matrices. F1-score reveal the error distribution between/among classes. The F1-score value is directly related to the degree of the representation accuracy of each class. The best F1-score a class can achieve is 1, the worst is 0. It was calculated using Equation (3).

$$F1score = 2 \times \frac{PA \times UA}{PA + UA} \tag{3}$$

where PA is producer's accuracy and UA is user's accuracy.

4 Results

In order to better identify, explore and understand the changes occurring on the agricultural areas, several statistical spatio-temporal observations of the polarized backscatter from the different fields or sections were extracted. Fourier time-series were created using mean backscattering coefficients. This was to increase the effectiveness of feature set consideration.

4.1 Time series analysis

4.1.1 Relationship between VV and VH

To better identify the crop types on the agricultural fields, the mean backscattering values were used to increase the effectiveness of feature set consideration. Figs. 3a–3f illustrate the trend variations in backscatter observed since the beginning of the period under investigation on the different fields for both VV and VH polarized backscatter. The profiles for each field were plotted, and the channel graphs reveal very similar patterns for all the VH polarized backscatter σ^0_{VH} (dB) values are lower than VV polarized backscatter σ^0_{VV} (dB) values. Each field reveals a unique trend dependent on the crop canopies and phenology, water content, and soil types. The activities reflected by both the polarized backscatter are very much comparable. Nevertheless, there are sometimes when the rate of changes from one date to another are not consenting to the same degree. However, no two fields are exhibiting the same profile. Crops planted on two fields at the same time, do not have identical profiles, the polarized backscatter trend captured is distinct. The scattering effects from the crops are different.

Generally, the σ^0_{VV} and σ^0_{VH} are positively correlated (Table 1); hence either of the profiles can be considered in the time series analysis to determine the trends.

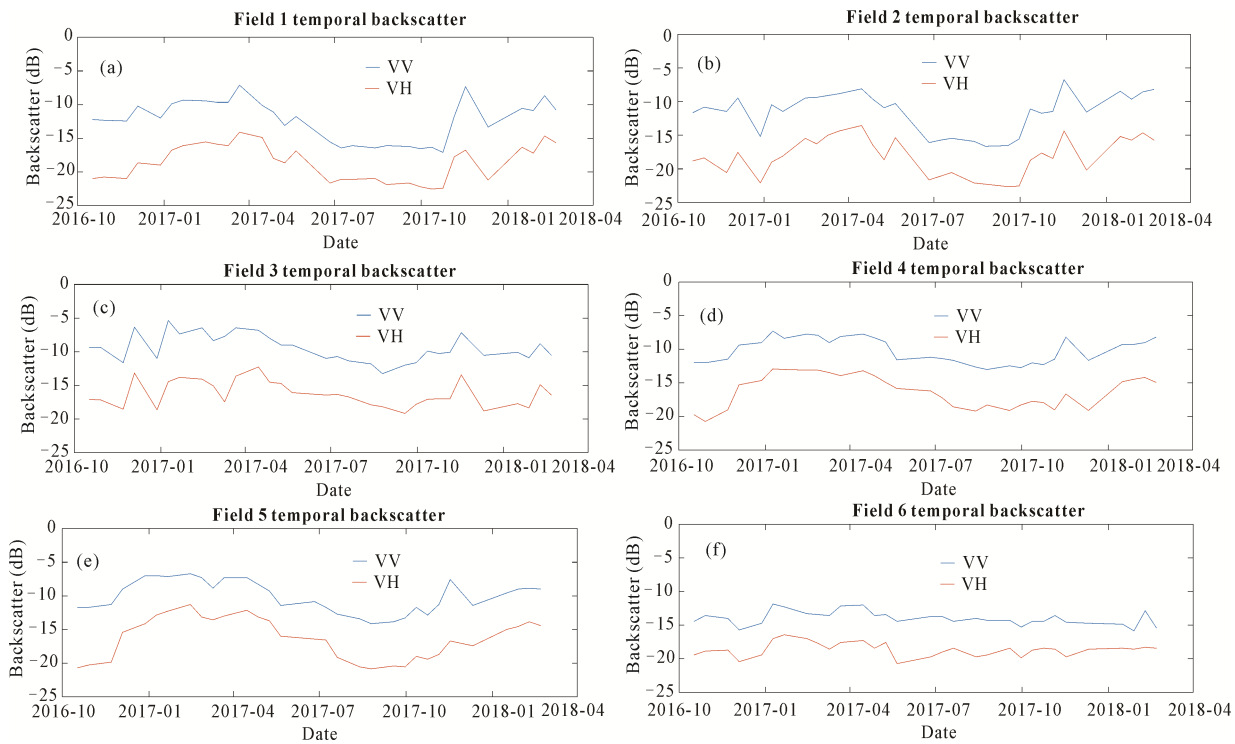

Fig. 3 Plots of both VV and VH polarized backscatter at selected fields at CIMMYT of Zimbabwe

Table 1 Correlation coefficients VV and VH polarized backscatter on fields

Field Number	Description	R^2
1	Soybean	0.8099
2	Maize	0.8647
3	Mixed	0.7172
4	Fallow	0.8039
5	Pasture	0.8361
6	Maize	0.7260

4.1.2 Fourier time series at CIMMYT

Fig. 4a illustrates selected smoothed time series plots of VV polarized backscatter on the different field parcels using Fourier series modeling. Fig. 4b shows time series plots of VH polarized backscatter on the field parcels. On both polarization backscatter profiles, the peak σ^0 (heading times) are between day 100 and day 200 of the investigation period and the second heading times (peak σ^0 values) are between day 450 and day 550. Crops are exhibiting different growth cycles on the time series. Unfortunately, during the period under investigation, there was no winter wheat grown.

For fields 1 and 2, in the first summer season, maize was planted, in winter, their corresponding troughs on the profiles are the lowest compared to the other fields which had a different crop. On Field 2 during the first summer, there was a late crop planted, but in the second summer, an earlier crop was planted. Profile of Field 6 is not similar to profiles of other cropping fields. It represents pasture/paddock, and the highest VV polarized backscatter values are around –12 dB and lowest are about –16 dB, the average becomes around –14 dB. There are not many fluctuations in the profile suggesting that irrigation is practiced. There exist some farm management be practiced in trying to maintain the same condition for the cattle feed.

Fig. 4 shows the multiple smoothed graphs using Fourier series modeling. The profiles using VV polarized backscatter are unique, hence the varying backscatter patterns represent characteristics of each field. It is possible to detect and differentiate the crops from each other at whatever growth stage unlike when using VH polarized backscatter. The VV polarized backscatter time series clearly shows plants in fields grown earlier or later than the others. Growth cycles are also clear enough to determine.

4.1.3 Fourier time series at Middle Sabi Estate

There are trend variations in the cropping patterns and crop cycles in different fields on a estate. Fig. 5 represents Fourier time series showing the multi-temporal dynamic patterns occurring within the estate for a 2-year period commencing January 2016 until January 2018.

Banana field (field 1) has the highest backscatter coefficients throughout, higher than all the sugarcane at different growth stages. Banana is a permanent crop and there is minimal fluctuation in the backscatter recorded. Fields 2, 3, 4, and 8 are sugarcane fields with different cropping cycles. Leafy vegetable-Tomato-Onion crop rotation is practiced on field 5. Water ponds have the lowest backscatter properties of the crops. Field 9 represents fallow fields for the whole duration under investigation. An increase in the backscatter at some point in time probably correspond to wind-pollinated plants, weeds, grass growing on the field, also water/moisture content influence the backscatter. Field 10 shows a tree plantation.

Sugarcane heading times/dates are distinct peaks on the smoothed time series as well as the growing cycles of sugarcane on different fields. Field 5 has a unique wave, with cycles lasting ±120 d. The crops being grown there are leafy vegetables, tomatoes, and onions. Thereby having more than triple-cropping intensity system per year.

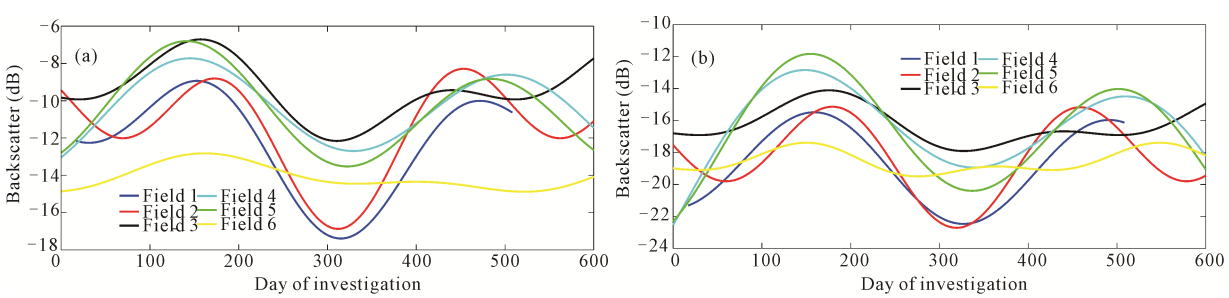

Fig. 4 Average polarized backscatter profiles of fields at CIMMYT of Zimbabwe. (a) VV and (b) VH

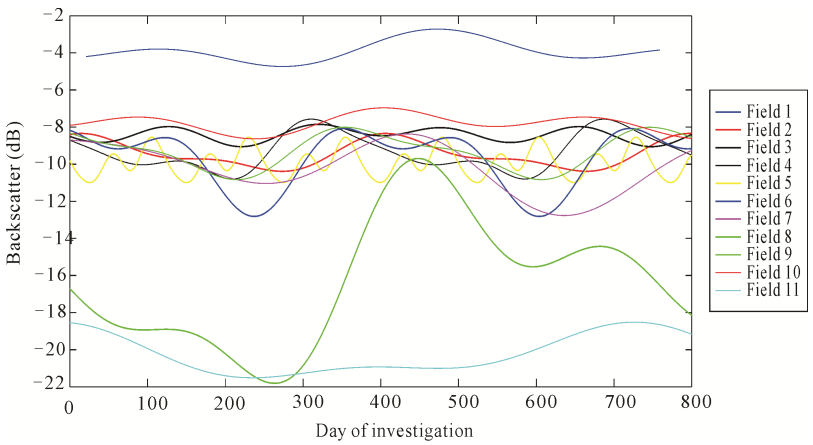

Fig. 5 Fourier series curve fitted VV polarized backscatter from fields at Middle Sabi Estate of Zimbabwe

4.2 Cropping calendar

Due to the crop rotation practiced at both sites, we divided the seasons into summer 1 and summer 2. Summer 1, planting is started around November up to February and harvesting is after day 200 (thus around early April) at CIMMYT. Summer 2 commences soon after day 400. There were no winter crops grown during the period under investigation. By the time this research was conducted, the second summer season was still on-going, hence the March 2018 imagery are not included since they were not yet available.

At Middle Sabi Estate, sugarcane has different harvesting times depending on their growing cycle. The leafy vegetables, tomato, and onion are grown and harvesting one after the other within a year. The banana growing cycle does not show much variation hence showing their perennial nature. During the period under investigation, the banana plants did not die, they were still growing and repeated their same cycle.

Trends on the different fields show different crop growth stages which makes it easier to differentiate them from each other. S1 time series allow crop type discrimination and development of cropping calendar at the various fields. Fewer images are required if the image acquisition is synchronized with the crop calendar (Toan et al., 1989; Ban and Howarth, 1999; Satalino et al., 2009; Moran et al., 2012). S1 SAR time series have great potential to produce cropping calendars on smaller scale farmlands. Crop type separability, C-band radar multiple images produce more accurate results than those achieved with a single C-band radar image (Satalino et al., 2009; Moran et al., 2012; Wang et al., 2010). The time series of σ^{o} (dB) can offer reliable information about crop cycles. The seasonal, temporal variations of backscatter can be considered as a function of crop growth.

4.3 Single date image classification

RF and *K*-means classification methods were applied on the 2 channels VV and VH polarized bands endeavoring to determine the various classes on some individual images collected on the different dates that have corresponding reference data. The RF classification results on single images were very poor with the highest overall accuracy of 46% obtained on image dated 9th February 2018 (Fig. 6a). The UAV reference image used was obtained on the 9th of February 2018 to rule out the fact of having used outdated reference samples.

K-means classification results on the same image dated 9th February 2018 achieved an overall accuracy of 40% (Fig. 6b). Both supervised and unsupervised classification did not produce satisfactory results. The SAR image contains information only in the form of intensity and texture (Chamundeeswari et al., 2007) but could not be segmented successfully into classes with accurate homogeneous properties. Nevertheless, both speckle and variation in the scattering coefficient with the incidence angle can affect the accuracy of pixel-based classifiers (Crawford and Ricard, 1998). Consequently, reasonable compensation procedures for these sources of variation in backscatter statistics are crucial to enable the production of an accurate classified map. The fewer the bands, the difficult it is to classify heterogeneous smallholder farming fields. Fewer polarization bands limit the ability to do pixel-based classification of single date SAR images.

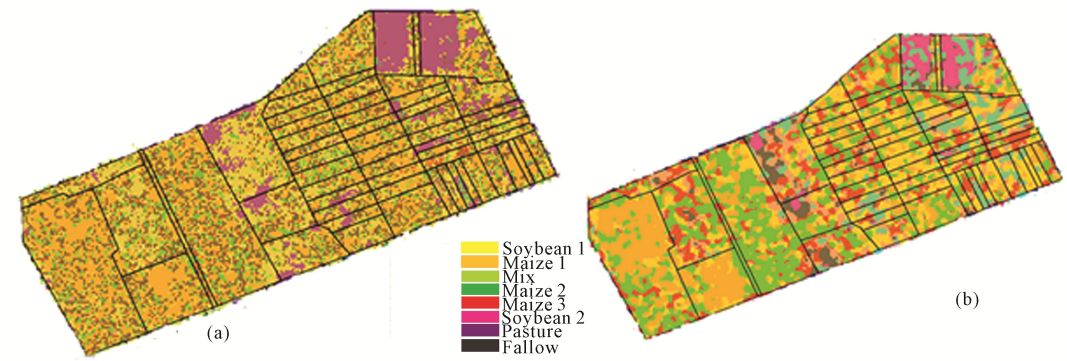

Fig. 6 Classified map of CIMMYT in Zimbabwe on 9th February 2018. (a) Random Forest (b) *K*-means

4.4 Crop rotation mapping

Each image contains vital information pertaining to the crop type but could not be fully retrieved by the classification of single date images since they have only two polarization bands. To overcome this limited ability to do digital classification on single date images with fewer polarization bands, we hereby classified the spatio-temporal image stacks to extract the spatio-temporal information embeded in the images based on the training and validation samples, and ancillary data.

The multi-temporal image stacks were classified using both *K*-means and RF algorithms. The overall accuracies obtained were 82% and 99% with kappa coefficients of 0.80 and 0.99, respectively at CIMMYT. Therefore, the RF classified image was adopted as the final map representing the crop rotation on the different fields. Fig. 7a shows crop rotation practiced on various fields. Since this site is a research and experimental location, the fields labeled mixed have different partitions with different crops under experiment hence why we considered them as mixed crop fields. There was no winter crop grown during the time of the investigation.

The Middle Sabi Estate's corresponding stacked images were also classified using both *K*-means and RF classifiers. The overall accuracies obtained were 65% and 95% with kappa coefficients of 0.53 and 0.95, respectively. Therefore, the RF classified image as adapted to be the final map representing the crop rotation determine on the different fields. Fig. 7b shows crop rotation practiced on the different fields as revealed by the classification process. The boundaries of the different fields are visibly distinct on the classified map. The fields are substantially larger than the fields at CIMMYT.

Post classification of combining classes was performed to have single classes of the same class type (sugarcane and fallow). And renaming of classes, the class name garden was changed to the crop rotation being practiced at the fields, thus leafy vegetable- tomato-onion.

4.5 F1 Test

Table 2 shows the producer's and the user's accuracies obtained from classifying the stacked images using RF algorithm. All classes performed well with F1 values higher than 99% for classes at CIMMYT. At Middle Sabi Estate, the classes also performed well with the least value of F1-score of 87%.

5 Discussion

This research aims at exploring the potential of mapping cropping patterns using C-band of S1 SAR data at small scale farming lands. The advantages of S1 SAR data are the fine spatial resolution best applicable to small fields, hence allowing the discovery of backscatter characteristics of the fields' pixels. Time series permits the detection of subtle changes that occur to the crops and fields, hence can be used to produce cropping calendars and detection of cropping patterns. The spatial distribution of cropping patterns makes it easier to understand the meaning of the land-use changes on the farmland at the different parcels growth rate, senescence and harvest rates can be determined using the multiple-temporal backscatter trend. There is an improved ability to differentiate crops type as well as differentiate crop phenologies. Crops grown at different times are exhibited in time series by waves lagging behind the earlier planted crops. The durations the growing period of crops

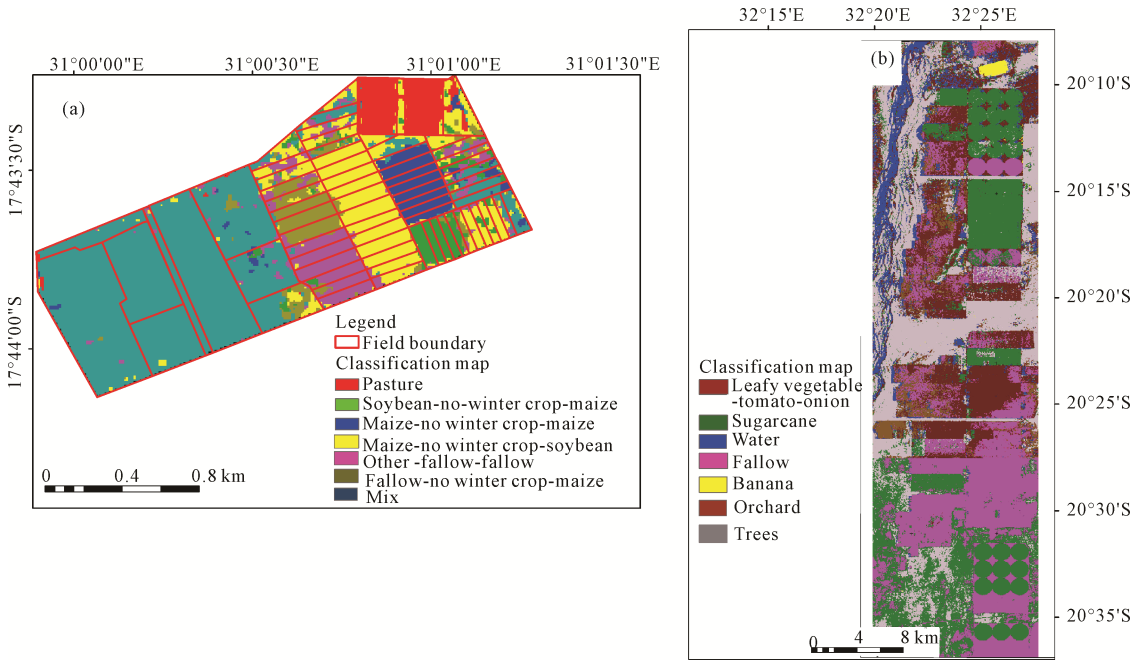

Fig. 7 Crop rotation classified maps at (a) CIMMYT and (b) Middle Sabi Estate of Zimbabwe

Table 2 F1-scores calculated from producer's and user's accuracies for random forest classified image for CIMMYT of Zimbabwe

Study location	Class	Producer's accuracy (%)	User's accuracy (%)	F1-score (%)
CIMMYT	Pasture	100.00	100.00	100.00
	Other-Fallow-Fallow	98.63	99.31	99.00
	Mixed	100.00	99.93	99.90
	Soybean-No winter crop-Maize	100.00	99.93	99.90
	Maize-No winter crop-Soybean	99.58	99.93	99.80
	Maize-No winter crop-Maize	100.00	100.00	100.00
Middle Sabi Estate	Banana	100.00	99.46	99.70
	Sugarcane 1	90.18	84.03	87.00
	Fallow 1	98.99	99.84	99.40
	Sugarcane 2	93.88	97.63	95.70
	Trees	98.68	99.17	98.90
	Orchard	99.38	87.35	93.00
	Leafy-vegetable-Tomato-Onion	99.59	99.64	98.60
	Sugarcane	100.00	100.00	100.00
	Fallow 3	100.00	85.27	92.00
	Fallow 4	88.82	99.62	93.90
	Water	99.28	95.87	97.50
	Fallow-No winter crop-Maize	99.28	100.00	99.60

can be detected on the time series. High backscatter values correspond to the greatest volume scatter caused by the canopy and branches of crops. Whereas the planting and germination of crops can be estimated from the time series. High deviations in backscatter suggest seasonality in agriculture activities. Temporal variations of polarized backscatter are regarded as a function of crop growth.

Upon classifying the stacked time series images, crop rotation maps are created and determined swiftly since each pixel provides a combination of characteristics contained by each pixel for the corresponding images

within the time series. Using Random forest, at CIMMYT, an overall accuracy of 99% was obtained, whereas at Middle Sabi Estate and overall accuracy 95% has been achieved. The high accuracy was achieved despite the size of the fields and farming area, environmental conditions or type of crops under investigation as long as the overall field size is bigger than the image pixel size. To produce a good classified map, the choice of classification algorithm must be dependent on the available training and validation samples one has regarding the area under investigation. The conclusion is based on the difference in sizes of study sites examined in this paper. The CIMMYT site is very small similar to an ordinary vegetable garden setup whereas Middle Sabi Estate is an intensive farming project for a group of small-scale.

The main limitation is in classifying single date images. The two channels considered could not provide enough complementary band information to derived a distinctive pattern necessary to produce a good classified image. Classification accuracy provided by single Synthetic Aperture Radar (SAR) data is generally considered not sufficient for operational crop mapping, hence a strong argument supporting the combined use of optical and SAR data is that the latter can provide additional and complementary information in terms of the canopy (Mattia et al., 2015). Conversely, there is also a need to determine the best time(s) of image acquisition for crop discrimination. The main advantage of classifying single date imagery is that it can capture the time when changes in field structures and arrangement occurred, which is a limitation of time series. Over the long term, rearrangements can be done on the ground due to various decisions by management. Some field boundaries are not permanent, the field parcels can be changed.

Nevertheless, good timing is crucial when choosing and classifying single date images. Proper planning of the dates of image acquisition and finding the optimal acquisition windows for the region of interest are, therefore crucial (Hütt and Waldhoff, 2018). Useful information can be missed when one uses the image captured on a particular day with less or more information than necessary, which may be misleading hence, not providing accurate information as required. According to Lin and Liu, (2016), the use of single imagery in classification might omit the information of some forests with short leaf-fall periods.

With the knowledge gained in this analysis, we recommend the application of mapping cropping patterns on both small-scale and large-scale farming areas. The next step will focus on determining how feasible it is to capture subtle changes in field boundaries as well as capturing the exact time the changes occurred from the time series data.

6 Conclusions

The main objective of this study was to explore the potential of mapping cropping patterns on smallholder scale farming land using Sentinel-1 SAR imagery. Two study locations, namely CIMMYT and Middle Sabi Estate of Zimbabwe were chosen due to the availability of data. Fourier time series was implemented to enable the detection of cropping patterns (cropping calendars and cropping systems) on the field parcels on the two locations. Random forest and *K*-means algorithms were used to classify stacked images to determine the crop rotations.

S1 SAR data can offer great potential when mapping cropping patterns on smallholder scale farming areas when working with multi-temporal images (time series). Fourier time series (spatio-temporal) profiles could be used to map cropping patterns on different small-scale agricultural fields since the multi-temporal observations can enable distinction of crop types and estimate the crop growth stages. CIMMYT practices a single cropping growing either maize or soybeans in summer. Middle Sabi Estate practices a single cropping on sugarcane whereas a triple cropping was observed on fields where leafy-vegetables, tomatoes, and onions are grown. However, there were subtle differences exhibited by crops of the same type but on different fields. The yearly sequential arrangement of both crops and fallow on each field could be identified. Crop planting dates and harvesting dates could also be estimated, patterns of early planted crops or late planted crops were exhibited by time series. Fourier time series permit identification of subtle changes occurring.

Random forest classification on respective multi-temporal image stacks comprising the time series enabled the identification and mapping of crop rotations on the small fields. High overall classification accuracies were achieved at CIMMYT attained 99%, and 95%

was obtained at Middle Sabi Estate. The classified maps synthesized are adopted as the crop rotation maps. High accuracy was achieved despite the size of the area, environmental conditions or type of crops under investigation. Classification of single date SAR image did not produce satisfactory results. The highest overall classification accuracy of 46% was obtained on the 9th February 2018 subset image when RF classification algorithm was implemented. *K*-means cluster method achieved an overall accuracy of 40% on the same image.

We, therefore, recommend the utilization of Sentinel-1 SAR multi-temporal data to spatially explicitly map cropping patterns of single-, double- and triple-cropping on both small-scale and large-scale farming areas to assist decision-makers pertaining to the food security and resource management issues.

Acknowledgement

We are grateful to Dr. Mainassara Zaman-Allah, Richard Makanza and Savemore Ngirazi for providing unmanned aerial vehicle (UAV) images.

References

Ban Y, Howarth P J, 1999. Multitemporal ERS-1 SAR data for crop classification: a sequential-masking approach. *Canadian Journal of Remote Sensing*, 25(5): 438–447. doi: 10.1080/07038992.1999.10874743

Bargiel D, 2017. A new method for crop classification combining time series of radar images and crop phenology information. *Remote Sensing of Environment*, 198: 369–383. doi: 10.1016/j.rse.2017.06.022

Bégué A, Arvor D, Bellon B et al., 2018. Remote sensing and cropping practices: a review. *Remote Sensing*, 10(1): 99. doi: 10.3390/rs10010099

Bharati P, De U K, Pal M, 2015. A modified diversity index and its application to crop diversity in Assam, India. *AIP Conference Proceedings*, 1643(1): 19–29. doi: 10.1063/1.4907421

Breiman L, 2001. Random forest. *Machine Learning*, 45(1): 5–32. doi: 10.1109/ACCESS.2019.2912807.

Chamundeeswari V V, Singh D, Singh K, 2007. Unsupervised land cover classification of SAR images by contour tracing. In: *Proceedings of 2007 IEEE International Geoscience and Remote Sensing Symposium.* Barcelona, Spain: IEEE, 547–550. doi: 10.1109/IGARSS.2007.4422852

CIMMYT, 2016. Our work. http://www.cimmyt.org/our- work/. Cited 22 March 2018.

Crawford M M, Ricard M R, 1998. Hierarchical classification of SAR data using a markov random field model. In: *Proceedings of 1998 IEEE Southwest Symposium on Image Analysis and Interpretation*. Tucson, AZ, USA: IEEE. doi: 10.1109/IAI.1998.666864

de Oliveira A T C, de Oliveira L T, de Carvalho L M T et al., 2009. Separabilities of forest types in amplitude-phase space of multi-temporal MODIS NDVI. In: *Proceedings of the Anais 14th Simpósio Brasileiro de Sensoriamento Remoto*. Natal, Brasil: INPE, 7.

Dimov D, Kuhn J, Conrad C, 2016. Assessment of cropping system diversity in the fergana valley through image fusion of landsat 8 and sentinel-1. *Proceedings of ISPRS Annals of the Photogrammetry*, *Remote Sensing and Spatial Information Sciences*. Prague, Czech Republic: ISPRS, 173–180. doi: 10.5194/isprsannals-III-7-173-2016

Doukkali F, 2017. Clustering using K-means algorithm. *Towards Data Science.* https://towardsdatascience.com/clustering-using-k-means-algorithm-81da00f156f6?gi=c1eec7743ec0. Cited 20 March 2018

Dzirutwe M, 2015. Zimbabwe takes tobacco road to agriculture recovery. https://www.yahoo.com/news/zimbabwe-takes-tobacco-road-agriculture-recovery-082633369-business.html. Cited 21 March 2018

Foody G M, McCulloch M B, Yates W B, 1994. Crop classification from c-band polarimetric radar data. *International Journal of Remote Sensing*, 15(14): 2871–2885. doi: 10.1080/01431169408954289

Forkuor G, Conrad C, Thiel M et al., 2014. Integration of optical and synthetic aperture radar imagery for improving crop mapping in Northwestern Benin, West Africa. *Remote Sensing*, 6(7): 6472–6499. doi: 10.3390/rs6076472

Heller E, Rhemtulla J, Lele S et al., 2012. Mapping crop types, irrigated areas, and cropping intensities in heterogeneous landscapes of southern india using multi-temporal medium-resolution imagery: implications for assessing water use in agriculture. *Photogrammetric Engineering & Remote Sensing,* 78(8): 815–827. doi: 10.14358/PERS.78.8.815

Hütt C, Waldhoff G, 2018. Multi-data approach for crop classification using multitemporal, dual-polarimetric TerraSAR-X data, and official geodata. *European Journal of Remote Sensing*, 51(1): 62–74. doi: 10.1080/22797254.2017.1401909

Jackson R D, 1984. Remote sensing of vegetation characteristics for farm management. In: *Proceedings of SPIE 0475*, *Remote Sensing: Critical Review of Technology*. Arlington: SPIE. doi: 10.1117/12.966243

Lee J S, Jurkevich I, Dewaele P et al. 1994, Speckle filtering of synthetic aperture aadar images: a review. *Remote Sensing Reviews*, 8(4): 313–40. https://doi.org/10.1080/02757259409532206

Le Toan T, Laur H, Mougin E et al., 1989. Multitemporal and dual-polarization observations of agricultural vegetation covers by X-band SAR images. *IEEE Transactions on Geoscience and Remote Sensing*, 27(6): 709–718. doi: 10.1109/TGRS.1989.1398243

Lin Sen, Liu Ronggao, 2016. A simple method to extract tropical monsoon forests using NDVI based on MODIS data: a case study in South Asia and Peninsula Southeast Asia. *Chinese*

Geographical Science, 26(1): 22–34. doi: 10.1007/s11769-015-0789-3

Lopes A, Nezry E, Touzi R et al., 1993. Structure detection and statistical adaptive speckle filtering in SAR images. *International Journal of Remote Sensing,* 14(9): 1735–1758. doi: 10.1080/01431169308953999

Marongwe L, Kwazira M, Jenrich et al., 2011. An African success: the case of conservation agriculture in Zimbabwe. *International Journal of Agricultural Sustainability*, 9(1): 153–161. doi: 10.3763/ijas.2010.0556

Martínez-Casasnovas J A, Martín-Montero A, 2003. Application of Landsat TM images to map long term cropping patterns. http://www.macaulay.ac.uk/workshop/remotesensing2004/JAMC_Full_paper.pdf. Cited 24 March 2018

Mattia F, Satalino G, Balenzano A et al., 2015. Sentinel-1 for wheat mapping and soil moisture retrieval. *Proceedings of 2015 IEEE International Geoscience and Remote Sensing Symposium.* Milan, Italy: IEEE, 2832–2835. doi: 10.1109/IGARSS.2015.7326404

McNairn H, Shang J L, 2016. A review of multitemporal synthetic aperture radar (SAR) for crop monitoring. In: Ban Y F (ed). *Multitemporal Remote Sensing: Methods and Applications*. Cham: Springer, 317–340. doi: 10.1007/978-3-319-47037-5_15

Moran S M, Alonso L, Moreno J F et al., 2012. A RADARSAT-2 quad-polarized time series for monitoring crop and soil conditions in Barrax, Spain. *IEEE Transactions on Geoscience and Remote Sensing*, 50(4): 1057–1070. doi: 10.1109/TGRS.2011. 2166080

Mukwada G, Manatsa D, 2013. Geospatial and temporal analysis of drought years in Zimbabwe, 1940–1999. *Geographia Polonica*, 86(4): 313–326. doi: 10.7163/GPol.2013.26

Nagraj G M, Karegowda A G, 2016. Crop mapping using SAR imagery: an review. *International Journal of Advanced Research in Computer Science*, 7(7): 47–52.

Nguyen D B, Clauss K, Cao S M et al., 2015. Mapping rice seasonality in the mekong delta with multi-year envisat ASAR WSM data. *Remote Sensing*, 7(12): 15868–15893. doi: 10.3390/rs71215808

Nyoungui E, Tonye E, Akono A, 2002. Evaluation of Speckle Filtering and Texture Analysis Methods for Land Cover Classification from SAR Images. *International Journal of Remote Sensing,* 23(9): 1895–1925. doi: 10.1080/01431160110036157

Ozdarici A, Akyurek A, 2010. A Comparison of SAR Filtering Techniques on Agricultural Area Identification. In: *ASPRS 2010 Annual Conference.* San Diego, USA. http://info.asprs.org/publications/proceedings/sandiego2010/sandiego10/Ozdarici. pdf. Cited 17 May 2019

Portnoi M D, 2017. *Methods for Sugarcane Harvest Detection Using Polarimetric SAR*. Stellenbosch: Stellenbosch University.

Satalino G, Mattia F, Le Toan T et al., 2009. Wheat crop mapping by using ASAR AP data. *IEEE Transactions on Geoscience and Remote Sensing*, 47(2): 527–530. doi: 10.1109/TGRS.2008.2008026

Sharma M P, Yadav M, Prawasi R et al., 2011. Cropping system analysis using remote sensing and GIS: a block level study of kurukshetra district. *ARPN Journal of Agricultural and Biological Science*, 6(10): 45–51.

Suresh G, Gehrke R, Wiatr T et al., 2016. Synthetic aperture radar (SAR) based classifiers for land applications in germany. *Proceedings of International Archives of the Photogrammetry, Remote Sensing and Spatial Information Sciences*. Prague, Czech Republic: ISPRS, 1187–1193. doi: 10.5194/isprs-archives-XLI-B1-1187-2016

Toringepi G, 2016. *The Contribution of Smallholder Agriculture Production to Food Security in Rural Zimbabwe: A Case Study of Masvingo Province*. South Africa: University of Fort Hare

Veci L, 2016. Sentinel-1 toolbox: TOPS interferometry tutorial. https://step.esa.int/docs/tutorials/S1TBX%20TOPSAR%20Interferometry%20with%20Sentinel-1%20Tutorial.pdf. Cited 20 March 2018

Wang Dan, Lin Hui, Chen Jinsong et al., 2010. Application of multi-temporal ENVISAT ASAR data to agricultural area mapping in the pearl river delta. *International Journal of Remote Sensing*, 31(6): 1555–1572. doi: 10.1080/01431160903475258

Wegmüller U, Werner A, Wiesmann A et al., 2016. Time-series analysis of sentinel-1 interferometric wide swath data: techniques and challenges. *Proceedings of 2016 IEEE International Geoscience and Remote Sensing Symposium.* Beijing, China: IEEE, 3898–3901. doi: 10.1109/IGARSS.2016.7730012

Yan Huimin, Xiao Xiangming, Huang Heqing et al., 2014. Multiple cropping intensity in China derived from agro-meteorological observations and MODIS data. *Chinese Geographical Science*, 24(2): 205–219. doi: 10.1007/s11769-013-0637-2